18th Australasian Wind Engineering Society Workshop
McLaren Vale, South Australia
6-8 July 2016

Performance analysis of a small wind turbine mounted inside a tall building

S.A H. Jafari, S. Hassanli and K.C.S. Kwok

Institute for Infrastructure Engineering
Western Sydney University, Penrith, NSW 2751,
Australia

Abstract

Using CFD simulations, a small conventional horizontal axis wind turbine (HAWT) Ampair 300 was installed in a confined flow space: through-building openings embedded at different levels of a tall building. The openings were located at 1/3, 1/2, 2/3 and 5/6 of the height of the building. The flow characteristics within the through-building openings when the building is exposed to a realistic wind profile have been investigated and applied to a single through-building opening including the small HAWTs. Four small HAWTs were located in the middle of each opening with a 3m × 3m cross-section area. Power generation and performance of the small turbines operating in the opening was investigated and compared with when installed in the free stream condition. It is shown that a confined space prevents flow from bypassing the turbines and increases the flowrate passing through it which results in power generation augmentation. For further flow enhancement, a compact diffuser was also integrated with the turbine and significantly enhanced its performance and power generation. This study shows that integration of wind turbine in a confined space with suitable design can enhance its performance and offers a potential location for integrating small wind turbines in an urban building.

Introduction

Interest in the design and development of small scale wind turbines for integration with urban buildings has increased world-wide during the last decades (Sharma and Madawala 2012, Drew et al. 2013). The main advantage is power generation at the point of use. However, there are hurdles which undermine wind turbine installations in the urban built environments such as: (i) lack of suitable area for medium-large size wind turbines; (ii) noise pollution in high wind velocity conditions; and (iii) relatively low power output and unreliable performance due to unfavorable urban wind conditions such as low wind velocity, continuously variable wind directions and high turbulence level (Ledo et al. 2011).

Toja-Silva et al. (2013) reported that horizontal axis wind turbines (HAWT) have better performance in flat-terrain applications, whereas in high-density building environments, vertical axis wind turbines (VAWT) are superior. Dayan (2006) showed that although the roughness of the terrain in urban environments can reduce the velocity and increase turbulence of the flow compared to open spaces, mounting turbines at high elevations on buildings may provide the perfect opportunity for onsite wind power harvesting. Many investigations have recently been done on advances in integration of small wind turbines in urban buildings (Ayhan and Sağlam 2012, Ishugah et al. 2014) and most of them have focused on roof-mounted wind turbines. Grant et al. (2008) proposed a roof-mounted ducted wind turbine, which uses pressure differentials created by wind flow around a building. Li et al. (2016) provided a performance assessment of four wind turbines installed in four openings in a tall building, Pearl River Tower, by conducting a 1:150 scale wind tunnel test and reported that the wind speeds in the openings can be intensified by an average factor of 1.90.

This study has investigated the integration of a small commercialized HAWT, Ampair 300 into ducted/confined spaces of a tall building using computational fluid dynamic (CFD) simulations. The proposed ducted/confined spaces are a couple of through-building openings embedded at both sides of four different levels of a 180 m high building at 60, 90, 120 and 150 m elevations from the ground. The building is exposed to a realistic wind condition (velocity and turbulence profile) based on the results achieved from a prior 1:400 scaled wind tunnel test (Kwok et al. 2014). A model of the scaled building with the selected openings was created under similar approach wind conditions and the flow characteristics have been investigated inside the openings. The CFD model of the HAWT has been located inside the openings with the identified flow characteristics. Performance of the HAWT is investigated and compared with the one located in a free stream condition and exposed to the same approach wind velocity. A compact diffuser was also integrated with the HAWT for performance augmentation and the enhancement is investigated.

CFD Model Setup

Building Geometry and Computational Model Setup

The dimensions of the building model (Melbourne, 1980) and the through-building openings are given in the Table 1. The openings are located at H/3 (60m), H/2 (90m), 2H/3 (120m) and 5H/6 (150m) where “H” refers to the building height, as shown in Figure 1. The windward and leeward side of the openings are open to the atmosphere. The windward openings are indicated with dashed lines in the enlarged building sketch.

A relatively small distance of 3H from inlet boundary to building is chosen to minimize the deterioration of the inlet profile due to the wall function problem (Blocken, Stathopoulos et al. 2007). This is sufficient in the case of a single building being modelled (Franke and Baklanov, 2007). The distance of lateral boundary is 3H. The distance of 10H is considered for the outlet from the building to allow for flow redevelopment behind the wake region. The computational domain was created with a blockage ratio of approximately 1% which is well below the recommended blockage ratio of 3% (Blocken, 2015).

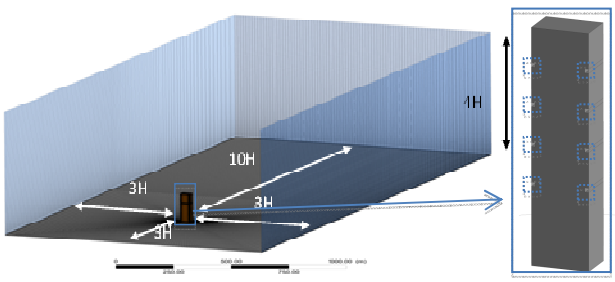

Figure 1. Building model with the through-building openings at four different elevations from the ground within the computational domain.

	Height (m)	Width (m)	Length (m)
Through-building opening	3	3	30
Building	180	30	45

Table 1. Dimensions of the building and through-building openings.

Based on the experimental data conducted by Kwok et al. (2014), the wind speed and turbulence intensity at the top of the building is about 12 m/s and 11%, respectively. The wind speed and turbulence intensity for the wind tunnel test and the CFD simulation at the target location is given in Figure 2 which shows an acceptable agreement. The discrepancy in turbulence intensity below 0.4H may arise from the wall function problem which has also been addressed by Blocken et al. (2007). Their remedial measures were implemented in the present study to minimize the discrepancy. The boundary conditions were considered as follows: symmetry condition at lateral boundaries, free slip condition at top boundary and outflow for outlet boundary.

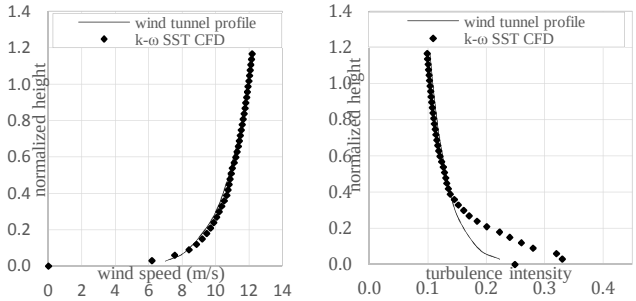

(a) (b)

Figure 2. Characteristics of wind flow at the target location.

Ampair 300 Model and Integration with the Building

The CFD model of the Ampair 300 has been developed and verified in a previous study (Jafari and Kosasih, 2014). This study integrated four Ampair 300, which each have a 1260mm diameter, in the middle of the through-building opening with 3m × 3m cross-section area, as shown in Figure 3(a). A compact diffuser with the dimensions indicated in Figure 3(b) is also integrated with the small HAWT for further flow enhancement. The rationale behind incorporating a diffuser with a wind turbine is to enhance the power generation by increasing the mass flowrate passing through the rotor. The diffuser creates a sub-atmospheric pressure region at its outlet and leads more wind through the rotor. This diffuser was selected since the configuration is compact and has been shown to be very effective/efficient (Jafari and Kosasih, 2014).

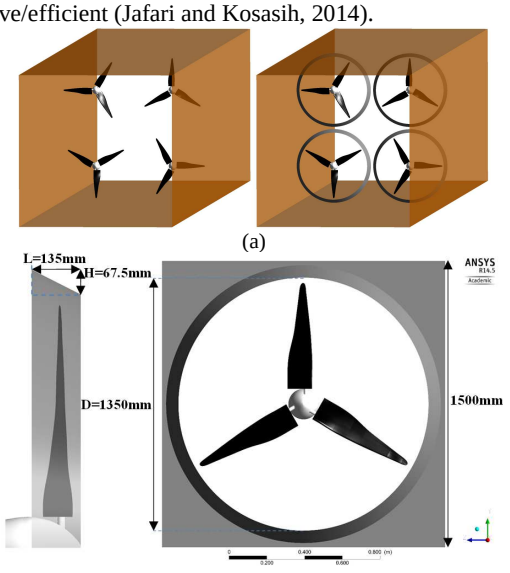

(a)

(b)

Figure 3. (a) HAWT and diffuser integrated model in the through-building opening and (b) Dimensions of the diffuser.

In order to save time and increase the accuracy of the results, the simulations have been done in two complementary phases. The first phase determined the mean velocity, pressure difference, Turbulent Kinetic Energy (TKE) and Turbulent Intensity (TI) throughout the openings by generating coarser grids along them and around the building. The second phase determined the resultant torque on the rotor by generating finer grids along the opening and around the rotor. The CFD model of the turbine and the openings were built using hybrid mesh including 1,150,000 structured and 650,000 unstructured grids in each quadrant of the opening while each quadrant includes one turbine in the middle. Structured mesh was built around the rotating disk shown in Figure 4(a), and very fine unstructured mesh was built within the rotating disk and on the rotor surface as shown in Figure 4(b). Gambit has been used for mesh generation in this study. The inlet boundary condition was imported from the results achieved in the first phase and the outlet boundary condition was set to outflow, since the details of the flow velocity and pressure are not known prior to the solution.

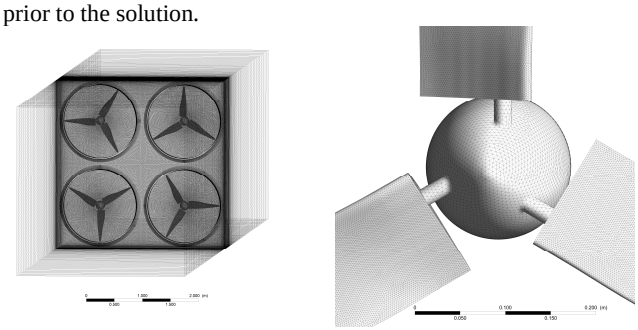

(a) (b)

Figure 4. (a) Structured mesh around the rotating disks, and (b) Very fine unstructured mesh on the rotor.

Solution Method

The k (TKE)-omega (SDR) SST (Shear Stress Transport) was used as the viscous model in this study. This model has been widely used in CFD simulation of rotating devices (Menter et al. 2006, Kirk-Davidoff and Keith 2008, Shives and Crawford 2010, Li et al. 2012, Lanzafame et al. 2013, Tavares Dias do Rio Vaz et al. 2014, Lanzafame et al. 2015, Wang et al. 2016). The viscous model was used to measure the torque (T) created on the rotor in each rpm (ω). The output power and the coefficient of performance (C_p) were then calculated from Equation (1). The C_p presents the ratio of power captured by the turbine (which equals torque T multiplied by the rotor rpm ω) to the total wind energy passing through the swept area:

$$C_p = \frac{P_{measured}}{P_{wind}} = \frac{T\,\omega}{0.5\,\rho\,AU^3} \quad (1)$$

Where ρ is the density of air, U is velocity and A is the effective area of the turbine. In the case of the bare turbine, A is the turbine swept area, whilst for the diffuser augmented turbine A is the diffuser outlet area. Hence, C_p needs to be calculated based on the outlet diameter of the diffuser.

The solver ran the model in transient condition using sliding mesh condition for the rotating disk by setting the adaptive time step to run the simulation for a minimum 1 sec. The CFD approach cannot automatically find the rotor's operational ω. Therefore, a series of simulations need to be performed in different ω to find the operational one (Jafari and Kosasih 2014). In particular, ω is gradually increased and the output power calculated at each step. Output power grows by increasing ω at lower ω values. However, at close to an optimum point, a further increase in ω results in decreasing the output power. The operational ω is ideally that optimum ω. In this study the rotor's ω was varied between 90 and 720 which at a wind velocity of 6 $m.s^{-1}$ resulted in a tip speed ratio (λ) of $1<\lambda<8$:

$$\lambda = \frac{r\omega}{U} \quad (2)$$

Where r is the radius of the rotor.

Results and Discussion

Velocity Analysis in Through-building openings

Figure 5(a) shows the velocity magnitude contour created on a cross-section of the building and along the through-building openings embedded at the selected elevations from the ground. The velocity magnitude contours show that the approach wind has been decelerated upon entering the openings but an acceptable velocity (6-7m.s^{-1}) is still available inside them. It is noteworthy that the velocity magnitudes and uniformity in the openings are very close to each other. The average flow characteristics in the openings are also measured and presented in Table 2. The measurements indicate that: (i) the maximum pressure difference is created at 2H/3 of the building, (ii) higher velocity is created inside the higher levels and (iii) higher turbulent intensity is observed inside the lower levels.

Figure 5(b) shows the plan view resultant velocity magnitude contour created in the openings at 120m elevation from the ground. It can be seen that the flow is very non-uniform at the inlet of the openings but the uniformity improved as the flow approaches the middle section. The major reason of the non-uniformity of the flow is the detachment/separation at the inlet. Moreover, the current results have been achieved when the building is normal to the incident wind and the detachment is likely to be intensified in other oblique wind conditions. Controlling the flow detachment/separation from the interior walls at the inlet can result in more uniform flow with higher velocity. Therefore, ongoing studies are being done on designing better layouts which preserves the favourable flow characteristics within the openings under variable wind incidence angles.

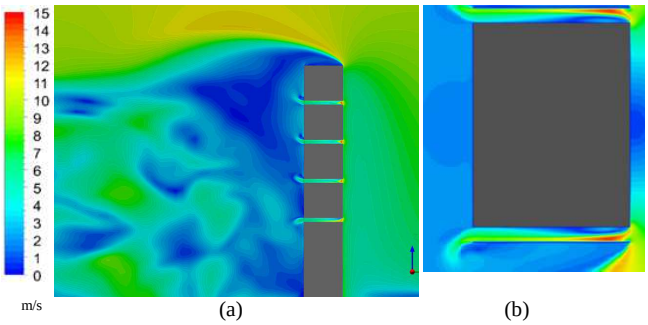

(a) (b)

Figure 5. Velocity magnitude contours (a) Around the building and along the through-building openings and (b) Along the openings at 120m elevation.

Height	Pressure Difference (Pa)	Mean Velocity (m.s^{-1})	TKE (m^2.s^{-2})	TI
60m	19.77	6.13	2.25	20%
90m	20.57	6.24	2.39	20%
120m	20.61	6.52	1.75	16.6%
150m	19.72	6.91	1.79	15.8%

Table 2. Flow characteristics in through-building openings at different elevations.

Pressure Analysis on Small Turbine Blades

Figure 6 shows the resultant pressures contours created on the high and low pressure sides of the HAWT blades. As can be seen the pressure difference created on the diffuser integrated turbine blades is the greater than the bare turbine. Therefore, the torque and power generation are expected to be greater. It can also be seen that the major pressure difference is due to the lower pressure created on the low pressure side of the diffuser integrated turbine. The reason is that the outlet area is greater than the inlet area which results in higher velocity and lower pressure at the inlet. The sub-atmospheric back pressure created at the inlet lowers the static pressure on the low pressure sides of the blades (Jafari and Kosasih 2014).

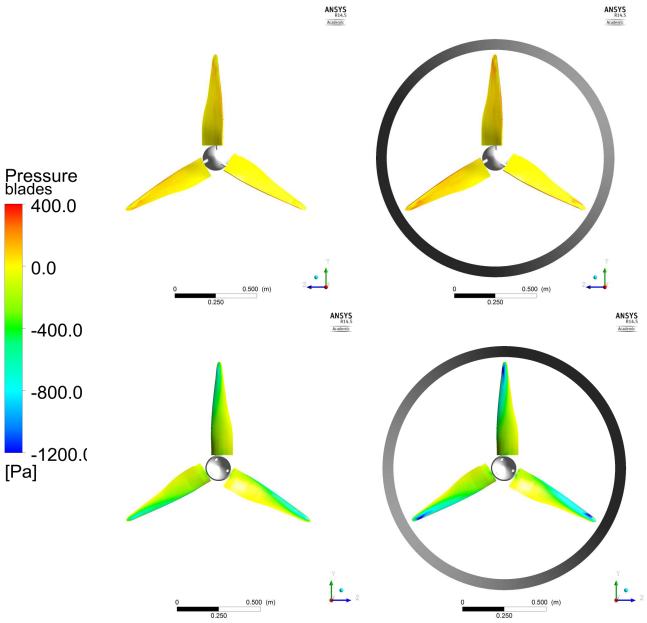

(a) (b)

Figure 6. Pressure contours on the high and low pressure sides of the HAWT blades (a) Without diffuser and (b) With diffuser attached

Coefficient of Performance and Power Generation

Figure 7 shows the C_p of the HAWT against λ when operating in the through-building opening with and without diffuser and compared with when operating in the free stream condition with the same velocity (6m.s^{-1}). As the C_p curves show, the performance has been increased 30% when operating in the opening and a further 30% when a diffuser is integrated. The C_p of the diffuser integrated HAWT operating in the opening has exceeded 0.5 while the C_p of the bare HAWT in free stream is around 0.25. The reason the C_p of the HAWT is increased in the opening is that the confined space prevents flow from bypassing the rotor and increases the flowrate passing through its space. The increased velocity creates a greater dynamic pressure and results in greater static pressure on the high pressure side of the blades. On the other hand, the diffuser creates a lower sub-atmospheric back pressure on the low pressure sides of the blades. The overall effect is around 100% increase in the C_p.

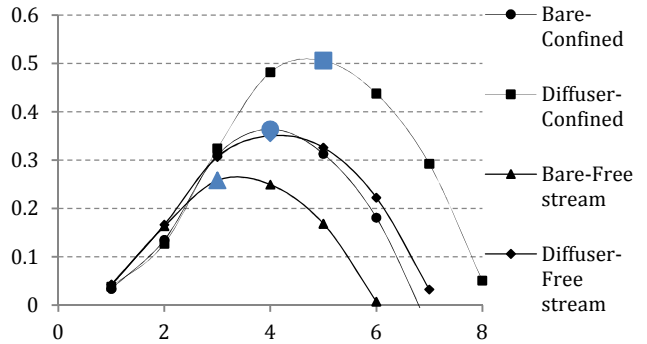

Figure 7 C_p calculated for the HAWT with and without diffuser in confined (through-building opening) and free stream conditions against λ.

Using the C_p achieved for each configuration and presented in Figure 7 and the wind power density (*WPD*) available in each

opening, power generation by the turbines can be calculated. The *WPD* shows the maximum power of a flow passing through a surface perpendicular to the flow direction divided by the total area of that surface, as defined in Equation (3).

$$WPD = \frac{1}{2}\rho U^3 \quad (3)$$

In this case, *U* refers to the mean velocity at different heights which are presented in Table 2.

Multiplying the *WPD* available in each opening by the effective area of the HAWT or the diffuser integrated model gives the maximum wind power passing through that effective area and, multiplying the result by the relevant C_p gives their actual power generation. Power generation by the HAWTs and their diffuser integrated model in each floor is calculated and presented in Table 3.

Height	Wind Power Density ($W.m^{-2}$)	Power Generation Bare (W)	Power Generation Diffuser (W)
60m	230.35	880	1,596
90m	242.97	928	1,684
120m	277.17	1,059	1,921
150m	329.94	1,260	2,286
Total		4,127	7,487

Table 3. Power generation by HAWTs and their diffuser integrated model installed in through-building openings in a tall building.

Conclusions

CFD model of Ampair 300, which is a small commercialized wind turbine, was integrated in a tall (180m) building inside the through-building openings embedded at 1/3, 1/2, 2/3 and 5/6 of the building height. The flow characteristics within the openings have been investigated when the building was exposed to a realistic wind profile. It has been shown that: (i) the maximum pressure difference is available at 2H/3 of the building, (ii) higher velocity is created inside the openings embedded at the higher levels and (iii) higher turbulent intensity is observed inside the openings embedded at the lower levels. Four small HAWTs were located in each opening with a 3m × 3m cross-section area. A compact diffuser was also integrated with the turbines for further flow enhancement. It was shown that a confined space prevents flow from bypassing the turbine and increases the flowrate passing through its rotor which results in power generation augmentation. The performance of the HAWT was increased 30% when operating in the opening and a further 30% when the diffuser was integrated. The C_p of the diffuser integrated HAWT operating in the opening exceeded 0.5 while the C_p of the bare HAWT in free stream is around 0.25. Power generation of these small turbines was also calculated and it was shown that these turbines can generate up to 7.5kW electricity with the selected layout design and approach wind profile.

References

Ayhan, D. and Ş. Sağlam (2012). "A technical review of building-mounted wind power systems and a sample simulation model." Renewable and Sustainable Energy Reviews 16(1): 1040-1049.

Blocken, B., 2015. Computational Fluid Dynamics for urban physics: Importance, scales, possibilities, limitations and ten tips and tricks towards accurate and reliable simulations. Building and Environment 91, 219-245.

Blocken, B., T. Stathopoulos and J. Carmeliet (2007). "CFD simulation of the atmospheric boundary layer: wall function problems." Atmospheric Environment **41**(2): 238-252.

Dayan, E. (2006). "Wind energy in buildings: Power generation from wind in the urban environment - where it is needed most." Refocus 7(2): 33-38.

Drew, D. R., J. F. Barlow and T. T. Cockerill (2013). "Estimating the potential yield of small wind turbines in urban areas: A case study for Greater London, UK." Journal of Wind Engineering and Industrial Aerodynamics 115(0): 104-111.

Franke, J. and Baklanov, A., 2007. Best practice guideline for the CFD simulation of flows in the urban environment: COST action 732 quality assurance and improvement of microscale meteorological models. Meteorological Inst.

Grant, A., C. Johnstone and N. Kelly (2008). "Urban wind energy conversion: The potential of ducted turbines." Renewable Energy 33(6): 1157-1163.

Ishugah, T. F., Y. Li, R. Z. Wang and J. K. Kiplagat (2014). "Advances in wind energy resource exploitation in urban environment: A review." Renewable and Sustainable Energy Reviews 37: 613-626.

Jafari, S. A. and B. Kosasih (2014). "Analysis of the power augmentation mechanisms of diffuser shrouded micro wind turbine with computational fluid dynamics simulations." Wind and Structures 19(2): 199-217.

Kirk-Davidoff, D. B. and D. W. Keith (2008). "On the Climate Impact of Surface Roughness Anomalies." Journal of the Atmospheric Sciences 65(7): 2215-2234.

Kwok, K., B. Samali, G. Hu and K. Tse (2014). "Wind-induced response reduction of a tall building with an innovative façade system."

Lanzafame, R., S. Mauro and M. Messina (2013). "Wind turbine CFD modeling using a correlation-based transitional model." Renewable Energy 52(0): 31-39.

Lanzafame, R., S. Mauro and M. Messina (2015). "HAWT Design and Performance Evaluation: Improving the BEM Theory Mathematical Models." Energy Procedia 82: 172-179.

Ledo, L., P. B. Kosasih and P. Cooper (2011). "Roof mounting site analysis for micro-wind turbines." Renewable Energy 36(5): 1379-1391.

Li, Q. S., Z. R. Shu and F. B. Chen (2016). "Performance assessment of tall building-integrated wind turbines for power generation." Applied Energy 165: 777-788.

Li, Y., K.-J. Paik, T. Xing and P. M. Carrica (2012). "Dynamic overset CFD simulations of wind turbine aerodynamics." Renewable Energy 37(1): 285-298.

Melbourne, W.H., 1980. Comparison of measurements on the CAARC standard tall building model in simulated model wind flows. Journal of Wind Engineering and Industrial Aerodynamics 6, 73-88.

Menter, F. R., R. Langtry and S. Völker (2006). "Transition Modelling for General Purpose CFD Codes." Flow, Turbulence and Combustion 77(1-4): 277-303.

Sharma, R. N. and U. K. Madawala (2012). "The concept of a smart wind turbine system." Renewable Energy 39(1): 403-410.

Shives, M. and C. Crawford (2010). Overall Efficiency of Ducted tidal current turbines. OCEANS 2010.

Tavares Dias do Rio Vaz, D. A., A. L. Amarante Mesquita, J. R. Pinheiro Vaz, C. J. Cavalcante Blanco and J. T. Pinho (2014). "An extension of the Blade Element Momentum method applied to Diffuser Augmented Wind Turbines." Energy Conversion and Management 87: 1116-1123.

Toja-Silva, F., A. Colmenar-Santos and M. Castro-Gil (2013). "Urban wind energy exploitation systems: Behaviour under multidirectional flow conditions—Opportunities and challenges." Renewable and Sustainable Energy Reviews 24: 364-378.

Wang, Y., X. Sun, X. Dong, B. Zhu, D. Huang and Z. Zheng (2016). "Numerical investigation on aerodynamic performance of a novel vertical axis wind turbine with adaptive blades." Energy Conversion and Management 108: 275